Joint probability analysis of storm surge and wave caused by tropical cyclone for the estimation of protection standard: a case study on the eastern coast of the Leizhou Peninsula and Hainan Island of China

Zhang Haixia[1,2,3,4], Cheng Meng[1,2,3,4], Fang Weihua[1,2,3,4]

5 [1] Key Laboratory of Environmental Change and Natural Disasters, Ministry of Education, Beijing Normal University, 100875, Beijing, China

[2] Academy of Disaster Risk Science, Faculty of Geographical Science, Beijing Normal University, 100875, Beijing, China

[3] Southern Marine Science and Engineering Guangdong Laboratory (Guangzhou), 511458, Guangzhou, Guangdong, China

[4] State Key Laboratory of Earth Surface Processes and Resource Ecology (ESPRE), Beijing Normal University, 100875, Beijing, China

Correspondence to: Weihua Fang (weihua.fang@bnu.edu.cn)

Abstract. The impact of natural hazards such as storm surges and waves on coastal areas during extreme tropical storm events can be amplified by the cascading effects of multiple hazards. Quantitative estimation of the marginal distribution and joint probability distribution of storm surges and waves is essential to understanding and managing tropical cyclone disaster risks.

15 In this study, the dependence between storm surges and waves is quantitatively assessed using the extreme value theory (EVT) and Copula function for the Leizhou Peninsula and Hainan Island of China, based on the numerically simulated surge heights (SHs) and significant wave heights (SWHs) for every 30 minutes from 1949 to 2013. The steps for determining coastal protection standards in scalar values are also demonstrated. It is found that, first, the generalized extreme value (GEV) function and Gumbel Copula function are suitable, respectively, for fitting the marginal and joint distribution characteristics of the SHs

20 and SWHs in this study area. Additionally, SH shows higher values as locations get closer to the coastline, and SWH becomes higher further from the coastline. Lastly, the optimal design criteria of SH and SWH under different joint return periods can be estimated using the non-linear programming method. This study shows the effectiveness of the bivariate Copula function in evaluating the probability for different scenarios, providing a valuable reference for optimizing engineering design criteria.

Keywords: Joint probability analysis, Storm surge and wave, Copula function, Tropical cyclone, Leizhou Peninsula and

25 Hainan Island

Deleted: copula

Deleted: copula

Deleted: copula

Deleted: Copula

1 Introduction

Tropical cyclone storm surges and waves could cause severe loss of life and property in offshore and coastal areas (Chen and Yu, 2017; Marcos et al., 2019; Wahl et al., 2015), and it is of great importance to quantify the intensity-frequency relationship of storm surges and waves, to understand the joint severity of multi-hazard extreme tropical cyclones (Zhang and Wang, 2021; Galiatsatou and Prinos, 2016).

In the past, many studies have analyzed the single hazard indicators for tropical cyclone storm surges and waves (Lin et al., 2010; Shi et al., 2020; Teena et al., 2012), often with observed time series data or with simulated results by numerical models (Petroliagkis et al., 2016; Bilskie1 et al., 2016; Huang et al., 2013; Papadimitriou et al., 2020). The intensity values of the surge height (SH) or significant wave height (SWH) of a specific return period can be estimated based on extreme value theory (Teena et al., 2012; Muraleedharan et al., 2007; Morellato and Benoit, 2010; Niedoroda et al., 2010). Accordingly, the estimated probabilities of single hazards, such as SH or SWH, have been widely applied in the protection standard design in coastal areas (Bomers et al., 2019; Perk et al., 2019; Lee and Jun, 2006).

However, strong storm surges and waves often occur concurrently during tropical cyclone events, which often cause greater impact than estimated only with a single variate due to the cascading effects of multi-hazards. For example, when high waves near the coast take place along strong storm surges, the overtopping and overflowing at sea dyke can lead to a large area of inundation and severe damage to coastal facilities (Rao et al., 2012; Hughes and Nadal, 2009; Pan et al., 2019). Similarly, rising sea levels due to storm surges would improve the probability of wave overtopping (Pan et al., 2013; Li et al., 2012). The concurrent interaction between storm surges and waves may cause the modeling of multi-hazards with significant uncertainties. Some studies have investigated the physical interaction of storm surges and waves through numerical simulation by coupling storm surge and wave models (Xie et al., 2016; Kimf et al., 2016; Brown, 2010) for specific events.

Statistical tools such as joint probability analysis have been used in multidimensional natural hazard assessment (Hsu et al., 2018). Since the Copula function does not restrict the marginal distribution function and can be relatively easily extended to multiple dimensions, it is often used to construct joint probability of multiple variates (Nelsen, 2006; Chen and Guo, 2019). There are a variety of applications with Copula function for double hazards, for example, rainfall and storm surge (Jang and Chang, 2022), wind and storm surge (Trepanier et al., 2015), and storm surge and wave (Corbella and Stretch, 2013; Wahl et

65   al., 2012).

In coastal protection standard design, it is essential to analyze and estimate the joint probability of SH and SWH. Chen et al. (2019) used the Copula functions to analyze the joint probability of extreme wave heights and surge heights at nine representative stations along China's coasts. Galiatsatou and Prinos (2016) investigated the joint probability of extreme wave heights and storm surges with time by a non-stationary bivariate approach. Marcos et al. (2019) statistically assessed the

70   dependence between extreme storm surges and wind waves along global coastal areas using the outputs of numerical models. Most previous joint probability studies on storm surges and waves mainly focused on location-specific rather than region-wide analysis. In addition, even with the joint probability of bivariate estimation, only an intercepted curve can be obtained since their probability is a three-dimensional surface. In addition, as the intensities of the bivariates and their simultaneous probability are three-dimensional surfaces, the cross-section at a given return period is a curve rather than a specific scale

75   value, so the joint probability of SHs and SWHs alone can not be used directly as a reference value for engineering design criteria. In order to obtain two specific scalars for SH and SWH, other constraints such as their preferred simultaneous return periods are needed (Xu et al., 2022).

In this study, we aim to explore the joint probability characteristics of tropical cyclone storm surges and waves for large coastal areas and to investigate the methods and steps for selecting the protection standard of sea dikes. Firstly, the marginal

80   distribution and Copula function of modeling nodes in the study area is fitted based on the long-term numerically simulated tropical cyclone SH and SWH from 1949 to 2013. Next, the optimal Copula functions are selected for every modeling node based on the Kolmogorov-Smirnov (K-S) test, AIC, and BIC. Then, the correlation between SH and SWH is quantified using the Copula function to calculate the probabilities under simultaneous, joint, conditional, and different-level combinations. The change in bivariate occurrence probability after increasing the engineering design criteria for the SHs and SWHs is

85   quantitatively assessed. Finally, with the maximum bivariate simultaneous return period as the objective function and the bivariate joint return period as the constraint, the optimum engineering design values of SHs and SWHs are solved by the non-linear programming method.

2 Study area and data

2.1 Best tracks of TCs

The best track dataset of historical TCs in the Northwest Pacific (NWP) is obtained from the Tropical Cyclone Data Center of the China Meteorological Administration (CMA). The CMA records in detail the location (longitude and latitude), time (year, month, day, hour), central minimum pressure, and 2-minute average near-center maximum sustained wind speed (MSW) for every 6-hour track point of each TC event since 1949 (Lu et al., 2021). The landfall of TCs in China is concentrated on the southeast coast, especially in the coastal areas of the South China Sea. Figure 1a shows the spatial distribution of the best track and maximum sustained wind speed of 86 historical TCs screened in this study from 1949 to 2013.
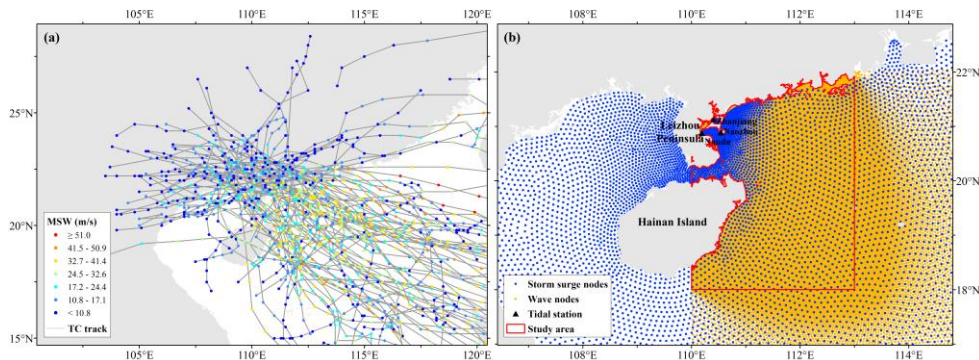
Figure 1: Best track and MSW of 86 TCs in this study from 1949 to 2013 (a) and the study area for the joint probability analysis of storm surges and waves of TCs (b).

2.2 Surge heights

The TC surge heights (SHs) dataset is obtained from the Ocean University of China, mainly through the ADvanced CIRCulation model (ADCIRC) simulations, which includes the SHs of 86 TCs affecting the eastern coast of the Leizhou Peninsula and Hainan Island from 1949 to 2013 (Liu et al., 2018; Li et al., 2016). The previous study provides a water depth map for the study area (Liu et al., 2018). The ADCIRC model integrates the effects of various boundary conditions and external forcing and uses triangular grids with different resolutions, making it more computationally efficient and applicable in

numerical simulations. The simulation results are the total water level after the superposition of the water gain caused by a tropical cyclone and astronomical tide, and the time step is 30 minutes.
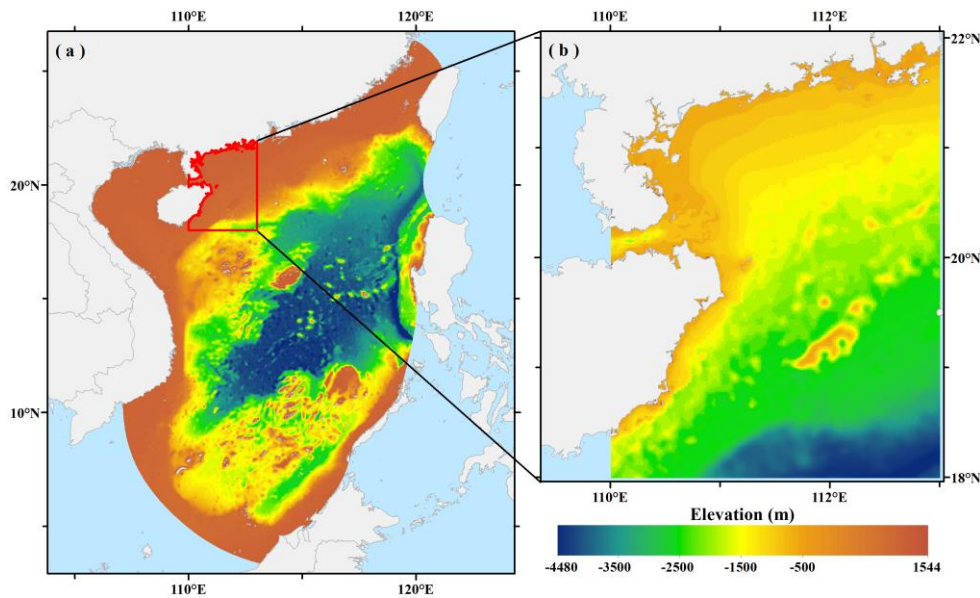
Figure 2: The bathymetry of storm surge modeling area (a) and study area (b).

To improve the simulation accuracy and computing speed of the hot spot area, the model adopts a triangular grid with nested small- and large-area grids, and the resolutions of different area grids are set in a gradual resolution range from 0.0039° to 0.3°. The calculation region for the large-area is 105.5° E-121.2° E and 3.3° N-26.4° N, and the calculation region for the small-area is 105.5° E-116.5° E and 14.7° N-23.1° N (Figure 2a). And a gradient resolution is used to set the resolution for different regional grids. In the large-area model, the whole large-area contains 9,331 triangular grid nodes and 18,068 triangles; the resolution of the shoreline in the area near Zhanjiang is 0.07°-0.1°, while the resolution in other area is about 1 km-2 km. In the small-area model, the whole small-area contains 41,153 triangular grid nodes and 79,889 triangles; the resolution of the shoreline near Zhanjiang port is 0.0039°-0.01, the resolution of the open boundary is set to 0.1°-0.3°. The full domain is driven

by atmospheric forcing at the surface and surge elevation inversed from the sea surface atmospheric pressure at the open boundary. ADCIRC computes water levels via the solution of the Generalized Wave Continuity Equation (GWCE), which is a combined and differentiated form of the continuity and momentum equations:

$$\frac{\partial^2 \zeta}{\partial t^2} + \tau_0 \frac{\partial \zeta}{\partial t} + Sp\frac{\partial \widetilde{J_\lambda}}{\partial \lambda} + \frac{\partial \widetilde{J_\varphi}}{\partial \varphi} - SpUH\frac{\partial \tau_0}{\partial \lambda} - VH\frac{\partial \tau_0}{\partial \varphi} = 0 \tag{1}$$

and the currents are obtained from the vertically-integrated momentum equations:

$$\frac{\partial U}{\partial t} + S_p U \frac{\partial U}{\partial \lambda} + V \frac{\partial U}{\partial \varphi} - fV = -gS_p \frac{\partial}{\partial \lambda}\left[\zeta + \frac{P_s}{g\rho_0} - \alpha\eta\right] + \frac{\tau_{s\lambda,winds} + \tau_{s\lambda,winds} - \tau_{b\lambda}}{\rho_0 H} + \frac{M_\lambda - D_\lambda}{H} \tag{2}$$

$$\frac{\partial V}{\partial t} + S_p U \frac{\partial V}{\partial \lambda} + V \frac{\partial V}{\partial \varphi} - fU = -g \frac{\partial}{\partial \varphi}\left[\zeta + \frac{P_s}{g\rho_0} - \alpha\eta\right] + \frac{\tau_{s\varphi,winds} + \tau_{s\varphi,winds} - \tau_{b\varphi}}{\rho_0 H} + \frac{M_\varphi - D_\varphi}{H} \tag{3}$$

where $H = \zeta + h$ is total water depth; ζ is the deviation of the water surface from the mean; h is bathymetric depth; $Sp = cos\varphi_0/cos\varphi$ is a spherical coordinate conversion factor and φ_0 is a reference latitude; U and V are depth-integrated currents in the $x-$ and $y-$ directions, respectively; $Q_\lambda = UH$ and $Q_\varphi = VH$ are fluxes per unit width; f is the Coriolis parameter; g is gravitational acceleration; Ps is atmospheric pressure at the surface; ρ_0 is the reference density of water; η is the Newtonian equilibrium tidal potential, and α is the effective earth elasticity factor; $\tau_{s,winds}$ and $\tau_{s,waves}$ are surface stresses due to winds and waves, respectively; τ_b is bottom stress; M are lateral stress gradients; D are momentum dispersion terms; and τ_0 is a numerical parameter that optimizes the phase propagation properties (Dietrich et al., 2012).

The boundary condition to force the surge in the subdomain is the time series of the water level on each boundary nodes, which includes both the tide elevation of 8 major constituents (M2, S2, N2, K2, K1, O1, P1, and Q1) in that area from OSU Tidal Prediction Software and the surge elevation extracted from the full domain results (Liu et al., 2018). Comparing the simulation values with the measured surge height at the observation sites, we discover that the absolute standard error is 47 cm, the relative standard error is 22%, and the simulation results are similar to the observed values in most cases. Thus, the dataset could be used to assess the hazard of TC storm surges. Figure 3a shows an example of the simulation results of the surge height of TC *Nasha* (ID:1117) at a specific moment.

2.3 Significant wave heights

The TC significant wave heights (SWHs) dataset is also obtained from the Ocean University of China, mainly through the

Simulating WAves Nearshore (SWAN) model, and includes the SWHs of 86 TC events affecting the study area from 1949 to 2013 (Li et al., 2016). The SWAN model has the advantage of high computational accuracy and stability and has been widely used in numerical simulations of offshore waters. The simulation results include indicators such as significant wave height, mean period, and wave direction, and the time step is 1 hour.

160 The model also uses a triangular grid with nested small- and large-area grids and gradual resolution, but the nodes' scopes and locations differ from those of the storm surge model. The calculation region for the large-area is 15° N-22° N, 110.5° E-118.5° E, which has a spatial step of 0.083° × 0.083°; the calculation region for the small-area is 21° N-21.2° N, 110° E-110.5° E, which has a spatial step of 0.0033° × 0.0033° (Figure 2b). The SWAN model includes land boundaries and water boundaries, which need to be set up separately. The model assumes that the land boundary does not generate waves and assumes that the

165 land boundary can fully absorb waves that cross or leave the shoreline. As the southern and eastern boundaries of the large-area model are open boundaries and are far from the shoreline, which is the focus of this study, the incoming wave energy at the open boundaries of the large-area model can be ignored, and the open boundary conditions for the small-area are calculated from the large-area model (Li et al., 2016). The governing equations of the SWAN model are as follows:

$$\frac{\partial N}{\partial t} + \frac{\partial}{\partial \lambda}[(c_\lambda + U)N] + cos^{-1}\varphi\frac{\partial}{\partial \varphi}[(c_\varphi + V)N\cos\varphi] + \frac{\partial}{\partial \theta}[c_\theta N] + \frac{\partial}{\partial \sigma}[c_\sigma N] = \frac{S_{tot}}{\sigma} \tag{4}$$

The wave action density $N(t, \lambda, \varphi, \sigma, \theta)$ is allowed to evolve in time (t), geographic space (λ, φ) and spectral space (with

170 relative frequencies σ and directions θ), (c_λ, c_φ) is the group velocity, (U, V) is the ambient current, and c_θ and c_σ are the propagation velocities in the θ- and σ- spaces, the source terms S_{tot} represent wave growth by wind (Dietrich et al., 2012).

Comparing the observed data of buoy stations with the simulated values reveals that the unstructured grid can well reflect the wave variation conditions in the sea. In addition, the mean absolute and root mean square errors of the simulated results of the

175 locally encrypted unstructured triangular grid are the smallest, indicating that the data can effectively reproduce the wave distribution during tropical cyclones. It shall be noted that the effect of sea level rise due to storm surge was not considered during the SWH simulation, which will influence the accuracy of SWHs, especially in intermedia and shallow water. In this paper, we choose the SWH as an indicator of tropical cyclone wave hazard. Figure 3b shows an example of the significant

180   wave height of TC *Nasha* (ID: 1170) at a specific moment.
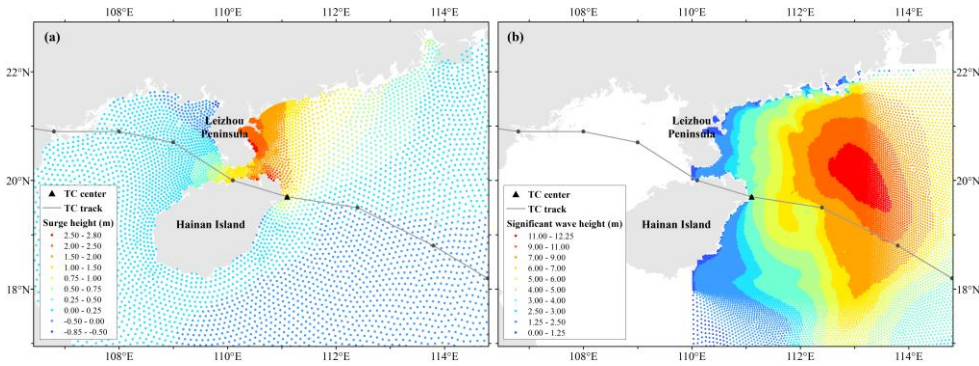
Figure 3: Distribution of surge height (a) and significant wave height (b) at a specific moment of TC *Nasha* (ID: 1117) (UTC:
2011.9.29 6:00:00)

2.4 Study area

185   Based on the location of the nodes of the triangular grid in the storm surge (Section 2.2) and wave datasets (Section 2.3), we

select the region with a dense distribution of both as the study area, and the finalized spatial range is 110°E - 113°E, 18°N -

22°N (Figure 1b). This area is located east of the Leizhou Peninsula and Hainan Island in the South China Sea, which is one

of the most frequently affected areas by tropical cyclones in China. Based on the dataset of surge height (SH) and significant

wave height (SWH) of tropical cyclones, we screen 86 historical tropical cyclones (TCs) events that simultaneously affected

190   the study area from 1949 to 2013 for joint probability characteristics analysis of storm surge and wave.

3 Methods

Sklar (Sklar, 1973) elucidates the role that Copula play in the relationship between multivariate distribution and their univariate

margins distribution, and states that any multivariate joint distribution can be described by a univariate marginal distribution

function and a couple describing the dependence structure between the variables (Nelsen, 2006). Let $F(x)$ and $G(y)$ be the

195   marginal distributions of x and y, C is the Copula, and $H(x,y) = C(F(x),G(y))$, where H is the bivariate joint

distribution function of x and y (Serinaldi, 2015). Therefore, the Copula function is widely utilized in multi-hazard joint

probability analysis of natural disasters (Chen et al., 2019; Lee et al., 2013).

3.1 Marginal function

The marginal function means that the probability density function (PDF) and cumulative distribution function (CDF) of the univariate are constructed by intensity-frequency analysis to reflect the probability of occurrence of the univariate at different intensities. The method is widely utilized in natural hazard assessments such as tropical cyclones, floods, droughts, and earthquakes. We select five commonly employed marginal functions for the annual extreme values fitting of tropical cyclone storm surges and waves, including the Gumbel, Weibull, gamma, exponential, and generalized extreme value (GEV) functions. In this study, the maximum likelihood method is used to estimate the function parameters, based on which the optimal marginal functions for SHs and SWHs are screened by the following steps: Firstly, the p-value of the K-S test is used to determine whether each node rejects the hypothesis that the samples obey a certain functional distribution. Secondly, the optimal function for each node is screened by the three metrics, AIC, BIC, and D-value of the K-S test. The smaller the AIC, BIC, and D-value of the K-S test, the better the goodness of fit, thus determining the optimal marginal function for each node. Finally, an optimal function is selected as the univariate marginal function for all nodes, and its PDF and CDF are fitted.

3.2 Bivariate Copula function

There are a variety of Copulas families, including Meta-elliptical Copulas (normal and t), Archimedean Copulas (Clayton, Gumbel, Frank, and Ali-Mikhail-Haq), Extreme Value Copulas (Gumbel, Husler-Reiss, Galambos, Tawn, and t-EV), and the other families (Plackett and Farlie-Gumbel-Morgenstern) (Chen and Guo, 2019). Among these Copulas, the Archimedean Copula is more popular for hydrologic applications. The commonly employed Archimedean Copula functions include Gumbel, Clayton, and Frank (Table 1), which are selected to analyze the joint probabilities of two variables, the SHs, and SWHs of a tropical cyclone. Then the maximum likelihood method is used to estimate the parameters of the Copula function. Next, we fit the goodness-of-fit of Copula functions for the tropical cyclone storm surge and waves at each node by the K-S test. According to the passing rate of the K-S test at the sample nodes, an optimal function is selected as the Copula function for all nodes of the two-dimensional variables, and the PDF and CDF are calculated.

Deleted: copula

Deleted: copula

Deleted: copula

Deleted: copula

Deleted: copula

Deleted: copula

Deleted: copula

Deleted: copula

Formatted: Font color: Text 1

Deleted: Table 1Table 1

Deleted: copula

Deleted: copula

Deleted: copula

Table 1 Formulas and parameter ranges for three types of bivariate Archimedean Copula functions.

Name of Copula	Bivariate Copula	Parameter θ
Clayton	$C_\theta(u,v) = [max\{u^{-\theta} + v^{-\theta} - 1; 0\}]^{-1/\theta}$	$\theta \in [-1, \infty)\backslash\{0\}$
Frank	$C_\theta(u,v) = -\dfrac{1}{\theta} log\left[1 + \dfrac{(e^{-\theta u} - 1)(e^{-\theta v} - 1)}{e^{-\theta} - 1}\right]$	$\theta \in R\backslash\{0\}$
Gumbel	$C_\theta(u,v) = exp\left[-\left((-log(u))^\theta + (-log(v))^\theta\right)^{\frac{1}{\theta}}\right]$	$\theta \in [1, \infty)$

Note: u and v are uniform (0,1) random variables (Nelsen, 2006).

3.3 Joint probability of storm surges and waves

3.3.1 Univariate return period

240 The return period (RP) indicates the period of natural hazard events, and it is a crucial indicator for quantifying the hazard level, which is widely utilized in hazard analysis. The formula for the return period of a single hazard indicator is as follows.

$$RP_X = \frac{E_L}{1 - F_X(x)} = \frac{E_L}{1 - P(X \le x)} \tag{5}$$

where RP_X is the return period of the univariate X; $F_X(x) = P(X \le x)$ is the marginal function of the univariate X; and E_L denotes the time interval of the sample series of the univariate X, the value is taken as 1 in this paper.

3.3.2 Bivariate probability and return period

245 Based on the Copula function, it can quantitatively estimate the probability of a multivariate being greater than a specified threshold. The bivariate probability refers to the likelihood that various conditions will occur simultaneously, and the bivariate return period refers to the average time interval required for multiple states to be simultaneously greater than a certain threshold. The definitions of three types of joint probabilities and return periods are given according to the univariate return period formula. The first type is when two variables simultaneously reach a given threshold, which will be defined as the simultaneous

250 probability $P_\cap$ (Eq. 6) and simultaneous return period $RP_\cap$ (Eq. 7). The second type is that at least one variable reaches a given threshold, which is defined as the joint probability $P_\cup$ (Eq. 8) and joint return period $RP_\cup$ (Eq. 9). The third type is the conditional probability $P_|$ (Eq. 10) and conditional return period $RP_|$ (Eq. 11), where when one of the variables reaches a

Deleted: copula

Deleted: copula

Deleted: 2

Deleted: 3

Deleted: 4

Deleted: 5

Deleted: 6

Deleted: 7

given threshold, the other variable also reaches a certain threshold. The formula is as follows (Serinaldi, 2015):

$$P_{\cap} = P\big((X > x) \cap (Y > y)\big) = 1 - P(X \leq x) - P(Y \leq y) + P(X \leq x, Y \leq y)$$

$$= 1 - F_X(x) - F_Y(y) + F_{X,Y}(x,y) \tag{6}$$

$$RP_{\cap} = \frac{E_L}{P\big((X > x) \cap (Y > y)\big)} = \frac{E_L}{1 - F_X(x) - F_Y(y) + F_{X,Y}(x,y)} \tag{7}$$

$$P_{\cup} = P\big((X > x) \cup (Y > y)\big) = 1 - P(X \leq x, Y \leq y) = 1 - F_{X,Y}(x,y) \tag{8}$$

$$RP_{\cup} = \frac{E_L}{P\big((X > x) \cup (Y > y)\big)} = \frac{E_L}{1 - F_{X,Y}(x,y)} \tag{9}$$

$$P_| = P\big((X > x)|(Y > y)\big) = \frac{P(X > x, Y > y)}{P(Y > y)} = \frac{1 - P(X \leq x) - P(Y \leq y) + P(X \leq x, Y \leq y)}{1 - P(Y \leq y)}$$

$$= \frac{1 - F_X(x) - F_Y(y) + F_{X,Y}(x,y)}{1 - F_Y(y)} \tag{10}$$

$$RP_| = \frac{E_L}{P\big((X > x)|(Y > y)\big)} = \frac{E_L \cdot \big(1 - F_Y(y)\big)}{1 - F_X(x) - F_Y(y) + F_{X,Y}(x,y)} \tag{11}$$

where $F_X(x)$ and $F_Y(y)$ are the marginal functions of the univariate X and Y, respectively, and $F_{X,Y}(x,y)$ is the joint distribution function of the two-dimensional variables (X,Y).

3.3.3 Combined scenario probability

265   To carry out the tropical cyclone storm surge and wave combination scenario simulation, we classify the SH and SWH into five classes (Table 2) by referring to the *Technical directives for risk assessment and zoning of marine disasters—Part 1: Storm Surge* (MNR, 2019) and *Part 2: Waves* (MNR, 2021). We calculate the bivariate probabilities for discretized hazard level combination scenarios based on the marginal and Copula functions of the storm surge and wave. The formula is as follows:

$$P_\& = P(x_1 < X \leq x_2, y_1 < Y \leq y_2)$$

$$= P(X \leq x_2, Y \leq y_2) - P(X \leq x_2, Y \leq y_1) - P(X \leq x_1, Y \leq y_2) + P(X \leq x_1, Y \leq y_1) \tag{12}$$

$$= F_{X,Y}(x_2, y_2) - F_{X,Y}(x_2, y_1) - F_{X,Y}(x_1, y_2) + F_{X,Y}(x_1, y_1)$$

Table 2 Hazard level classification criteria for combined scenarios of tropical cyclone surge height and significant wave height

Hazard level	Surge height (m)	Significant wave height (m)
I	[2.5, +∞)	[14.0, +∞)
II	[2.0, 2.5)	[9.0, 14.0)

III	[1.5, 2.0)	[6.0, 9.0)
IV	[1.0, 1.5)	[4.0, 6.0)
V	[0.0, 1.0)	[0.0, 4.0)

3.4 Design of protection standards for storm surge and wave

3.4.1 Probability changes under increased storm surge and wave protection standards

In actual engineering protection design, if the protection standards of SH and SWH are appropriately increased or decreased, it can change the simultaneous bivariate probability $P_\cap$, joint bivariate probability $P_\cup$, and conditional bivariate probability $P_|$. In this paper, we try to estimate the change value of the bivariate probability by raising the return period of storm surge or wave. The formula is as follows:

$$P_{d_\cap} = P\big((X > x_2) \cap (Y > y)\big) - P\big((X > x_1) \cap (Y > y)\big)$$

$$= P(X \le x_2, Y \le y) - P(X \le x_2) - P(X \le x_1, Y \le y) + P(X \le x_1) \tag{13}$$

$$= F_{X,Y}(x_2, y) - F_X(x_2) - F_{X,Y}(x_1, y) + F_X(x_1)$$

$$P_{d_\cup} = P\big((X > x_2) \cup (Y > y)\big) - P\big((X > x_1) \cup (Y > y)\big) = P(X \le x_1, Y \le y) - P(X \le x_2, Y \le y) \tag{14}$$

$$= F_{X,Y}(x_1, y) - F_{X,Y}(x_2, y)$$

$$P_{d_|} = P\big((X > x_2)|(Y > y)\big) - P\big((X > x_1)|(Y > y)\big)$$

$$= \frac{P(X \le x_2, Y \le y) - P(X \le x_2) - P(X \le x_1, Y \le y) + P(X \le x_1)}{1 - P(Y \le y)} \tag{15}$$

$$= \frac{F_{X,Y}(x_2, y) - F_X(x_2) - F_{X,Y}(x_1, y) + F_X(x_1)}{1 - F_Y(y)}$$

where $P_{d_\cap}$, $P_{d_\cup}$, and $P_{d_|}$ are the changes of the simultaneous probability $P_\cap$, the joint probability $P_\cup$, and the conditional probability $P_|$ after the univariate return period is raised; and x_1 and x_2 are the intensity values of variable X for different return periods, respectively, where $x_2 > x_1$.

3.4.2 Design storm surge and wave criteria for joint return period scenarios

Based on the binary Copula function, the bivariate joint probability of extreme storm surges and waves under different joint return periods is available. In order to achieve the optimal protection effects, it is natural that we need to set the maximum

bivariate simultaneous probability of SH and SWH as target functions (Eq. 16) and use joint probability as constraints (Eq. 17).

$$max\ \{P_\cap\} = min\ \{RP_\cap\} = min\left\{\frac{E_L}{P\big((X>x)\cap(Y>y)\big)}\right\} = min\left\{\frac{E_L}{1-F_X(x)-F_Y(y)+F_{X,Y}(x,y)}\right\} \quad (16)$$

$$\left\{\begin{array}{l} K = RP_\cup = \dfrac{E_L}{P\big((X>x)\cup(Y>y)\big)} = \dfrac{E_L}{1-P(X\le x, Y\le y)} = \dfrac{E_L}{1-F_{X,Y}(x,y)} \\ \qquad\qquad x\in(0,40) \\ \qquad\qquad y\in(0,40) \end{array}\right. \quad (17)$$

According to the non-linear programming method (Bazaraa et al., 2006), for a combined event of extreme SHs and SWHs, a series of (x,y) shall be iterated to minimize $P\{X>x, Y>y\}$ for a given joint return period to obtain the best cost-benefit effect. Therefore, the optimal values of SH and SWH can be solved, as illustrated in Figure 4. Since we have the estimation of the joint probability for the study area instead of some specific locations, the optimal design criteria for all the eastern coasts of the Leizhou Peninsula and Hainan Island can be estimated.

Figure 4: Diagram of determining SH and SWH based on their joint and simultaneous return periods (red curves are joint return periods (RP$_\cup$), black curves are simultaneous return periods (RP$_\cap$), and black dots (x, y) is the optimal SH and SWH).

Deleted: are

4 Results and discussion

4.1 Optimal marginal function

395 Since the different densities and locations of the triangular grids in the storm surge and wave models, we use the storm surge triangular grid nodes as the benchmark and the wave node closest to each storm surge node as the wave simulation result based on the nearest neighbor method. Therefore, a dataset of storm surges and waves with the same number and location of nodes is reconstructed, containing 1665 nodes in the study area.

In this paper, based on the reconstructed storm surge and wave simulation results of historical TC events, we calculate each

400 node's annual extreme values of SH and SWH. Firstly, the time series of the bivariate annual maximum value for all nodes are fitted with five marginal functions, including Gu

Deleted: node's

mbel, Weibull, gamma, exponential, and generalized extreme value (GEV). Next, the p-value of the K-S test is used to determine whether the hypothesis that the sample obeys a certain theoretical distribution is rejected. Then, we count the number of nodes passing the K-S test for each function and their percentage of all nodes. Finally, the number of nodes and their

405 percentage of each function being selected as optimal is calculated according to the steps for optimal function selection in Section 3.1 (Table 3).

Table 3 Frequency and percentage of five functions passing the K-S test and the optimal function for all nodes of SH and SWH

Marginal function	Surge height				Significant wave height			
	Frequency of K-S test passed	Percentage of K-S test passed (%)	Frequency of optimal function	Percentage of optimal function (%)	Frequency of K-S test passed	Percentage of K-S test passed (%)	Frequency of optimal function	Percentage of optimal function (%)
Gamma	1508	90.57	183	10.99	1464	87.93	159	9.55
Exponential	1567	94.11	216	12.97	1076	64.62	95	5.71
Gumbel (right)	1615	97.00	350	21.02	1629	97.84	149	8.95
Weibull (max)	1469	88.23	416	24.98	300	18.02	494	29.66
GEV	1665	100.00	500	30.04	1657	99.52	768	46.13
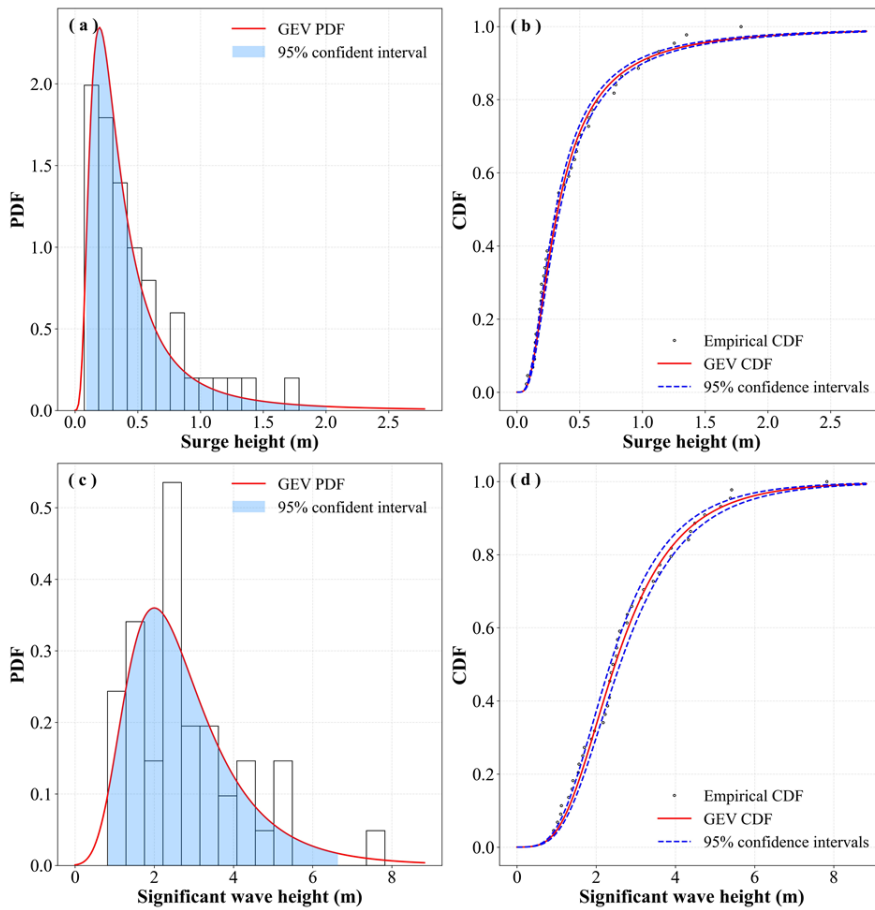
410

Figure 5: Fitting results of the PDF and CDF of the SH and SWH based on the GEV function (using node (110.5142° E, 20.2768° N) as an example)

Based on the statistical results, it is found that for fitting the SH, the K-S test of the GEV function had the highest no-rejection rate of 100%, and the corresponding optimal ratio was 30.04%, so GEV is set as the optimal marginal function in this study.

415   For SWH fitting, the number of nodes with no rejection in the K-S test of the GEV function is 1657, accounting for 99.52%

of the total number of nodes, and the corresponding percentage of preferences is also higher than that of other functions. We apply the GEV function to fit the marginal function of the SH and SWH at all nodes and calculate the PDF, CDF, and RP. Figure 5 shows an example of the PDF and CDF of the SH and SWH for a given node.

4.2 Distribution of univariate return periods

420   Based on the univariate return period formula (Eq. 5), the SH and SWH are estimated for six typical return periods of 5-year, 10-year, 20-year, 50-year, 100-year, and 200-year at all nodes. To analyze the distribution characteristics of the univariate return period in this study area, we chose the cubic spline interpolation method to interpolate the intensity values at each node with different return periods into a raster with a resolution of 1 km (Figure 6 and Figure 7).

As shown in Figure 6, the SH shows a significant increasing trend as it approaches the coastline. SHs along the eastern coast
425   of the Leizhou Peninsula are higher than most other regions. Frequent TC events, TC moving direction (Figure 1), and pocket-shaped coastal topography (Figure 2) are all favorable factors to water accumulation in this area. Another area with high SHs is located to the east of Hainan Island. Besides frequent TCs, this area is at the transition zone from the continental shelf to the continental slope, where bathymetry changes rapidly and can bring strong storm surges easily.
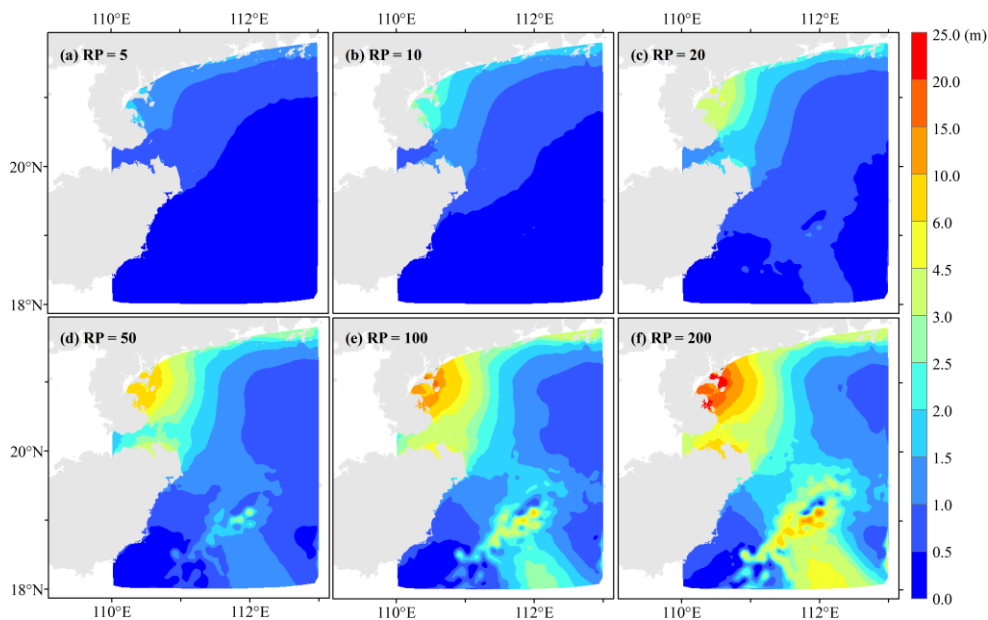
Figure 6: Spatial distribution of surge heights of tropical cyclones for six typical return periods

As shown in Figure 7, the SWHs near the shore are generally smaller than that in the open sea, and there is a significant decreasing trend in SWH as it gets closer to the coastline. This is mainly attributed to the shallow shore depth, island obstruction, wave breaking, and seabed friction attenuation. Among them, the SWHs in the eastern Leizhou Peninsula are lower than that of other seas, which is mainly influenced by the curved depressed coastline and the topography of the shore section. The SWHs are influenced by the frequency, duration, and intensity of TCs, so the SWH is higher in the east and south of Hainan Island than in the north. In addition, the east side of Hainan Island from the continental shelf to the continental slope causes a wave-breaking effect and dissipation caused by the dramatic change in seafloor topography height, which results in a more significant gradient in SWH. In addition, it shall be noted that errors may be introduced during the estimation of SWHs with GEV due to the limited number of TC events.
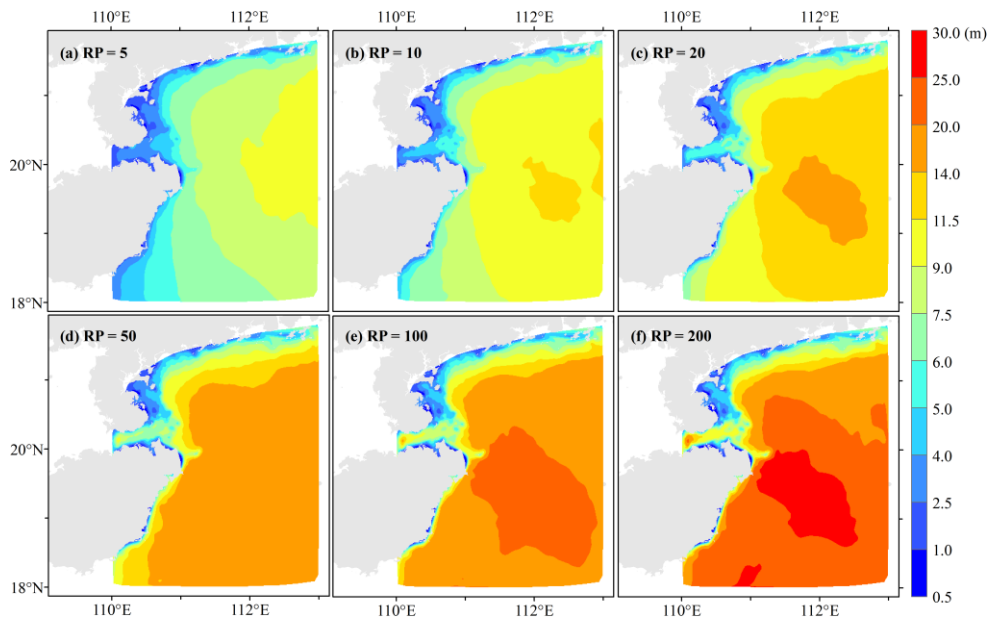
Figure 7: Spatial distribution of significant wave heights of tropical cyclones for six typical return periods

4.3 Optimal Copula function

The optimal GEV function is utilized as the marginal function for the TC storm surges and waves, based on which three Copula

620 functions are applied to the bivariate joint fitting of 1665 nodes. The function parameters are fitted by the maximum likelihood

method, and the K-S test is used to determine whether the hypothesis that the sample obeys a certain functional distribution is

rejected. Next, we count the number of nodes that pass the K-S test for the three types of Copula functions and their percentage

of the total number of nodes (Table 4). The statistical results show that the number of nodes passing the K-S test for the Gumbel

Copula function is 1603, accounting for 96.28% of all nodes, so it is used as the optimal Copula function in this study. The

625 Gumbel Copula function is applied to the bivariate joint fitting of SH and SWH for all nodes, and the PDF and CDF are

calculated.

Table 4 Frequency and percentage of three Copula functions passing the K-S test for all nodes of surge height and significant wave height of tropical cyclones

Copula function	Frequency	Percentage (%)
Clayton	486	29.19
Frank	1398	83.96
Gumbel	1603	96.28

4.4 Distribution of bivariate probabilities and return periods

Based on the optimal marginal function and Copula function, we calculate $RP_\cap$, $RP_\cup$, and $RP_|$ of SHs and SWHs. In addition, based on the formula of bivariate probability (Eq. 6 and Eq. 8), $P_\cap$ and $P_\cup$ of SH and SWH are calculated for all nodes with a combination of 10-year, 20-year, 50-year, and 100-year return period. To analyze the distribution characteristics, $P_\cap$ and $P_\cup$ for different combinations of return periods at each node are interpolated into a raster with a resolution of 1 km using the cubic spline interpolation method (Figure 8 and Figure 9).

The simultaneous bivariate probability $P_\cap$ gradually decreases as the return period of SH or SWH increases (Figure 8). Overall, the closer to the coastline, the higher $P_\cap$. $P_\cap$ is greatest when the return period of SH and SWH is 10-year, which is higher than 0.05. $P_\cap$ is the smallest for SH and SWH of 100-year return period, which is generally lower than 0.009.
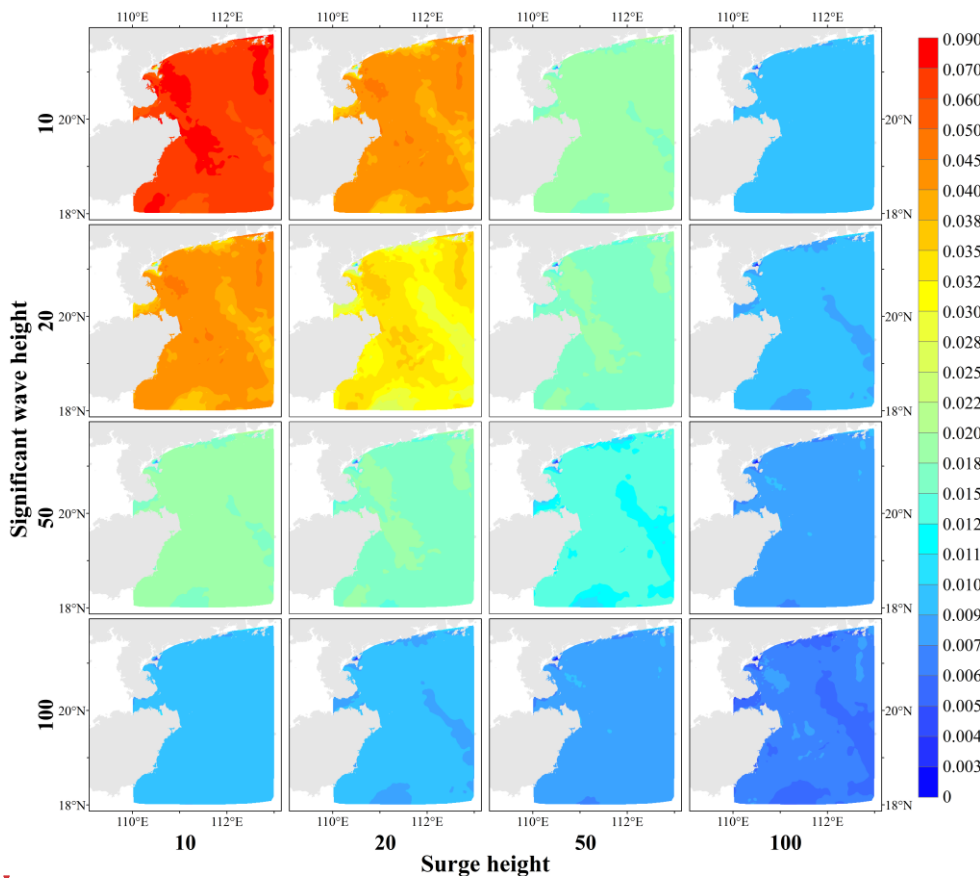
Figure 8: Simultaneous probabilities of combined scenarios with four typical return periods for surge height and significant wave heights of tropical cyclones

665   The joint bivariate probability $P_{\cup}$ of SH and SWH is higher than $P_{\cap}$, and it gradually decreases with an increasing return period of the two hazard indicators (Figure 9). Overall, the closer to the coastline, the higher $P_{\cup}$. $P_{\cup}$ is highest when the return period of SH and SWH is 10-year, which is greater than 0.13 overall. $P_{\cup}$ is smallest when the return period for SH and SWH is 100-year, which is less than 0.015. When the return period of SH or SWH is 50-year or 100-year, the regional variation
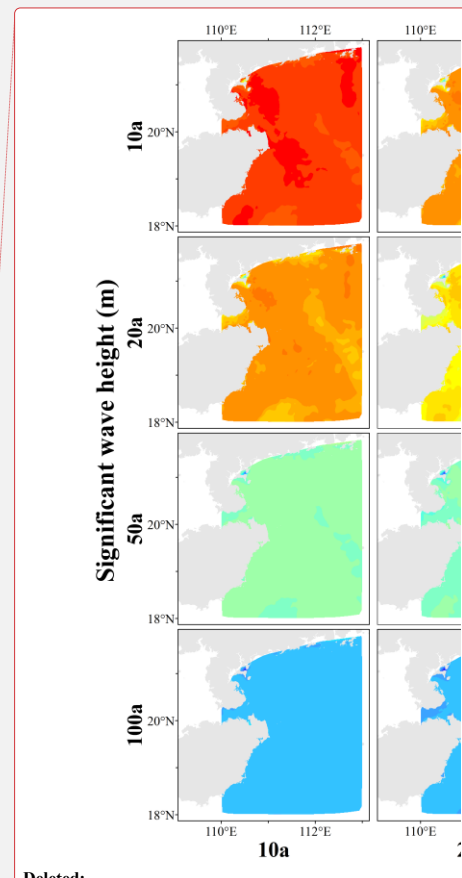
in P_U are relatively small.
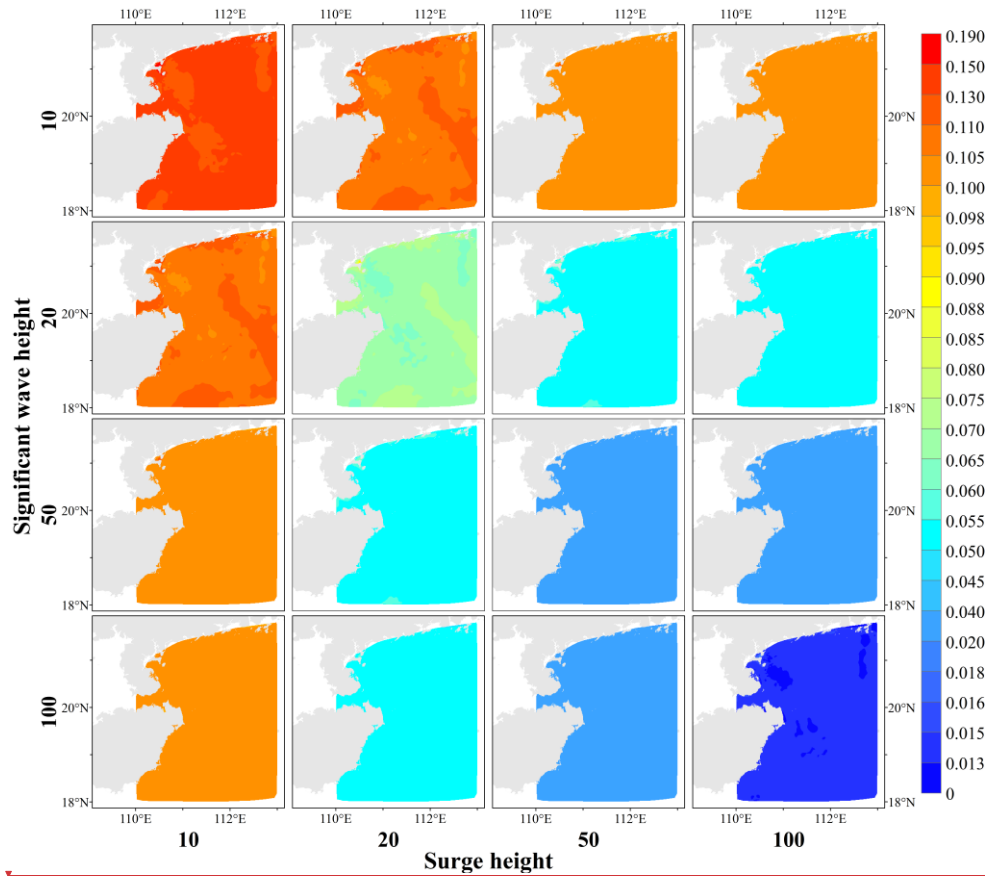
Figure 9: Joint probabilities of combined scenarios with four typical return periods for surge height and significant wave heights of tropical cyclones
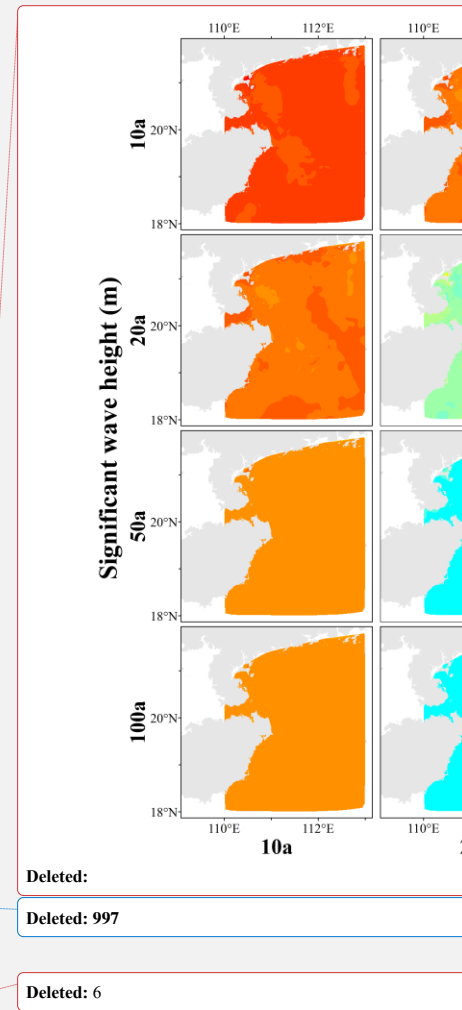
680 Based on the formula of conditional bivariate probability $P_|$ (Eq. 10), we calculate $P_|$ for all nodal univariates with different return periods for the other variable in four return periods, interpolate them into 1 km raster data using cubic spline interpolation. According to the formula, the calculation results are consistent when the positions of the variables are swapped. Therefore,

only $P_|$ for the four return periods of SH in different wave return periods are shown in this paper (Figure 10). When the SWH is a specific return period, $P_|$ gradually decreases as the return period of the SH increases. Under the condition that the return period of SWH is 10-year, $P_|$ for SH with a return period of 10-year are concentrated between 0.55 and 0.75, and $P_|$ is generally less than 0.08 if the return period for SH is 100-year. When the return periods of SWHs and SHs are equivalent, the

690 $P_|$ is concentrated between 0.55 and 0.75.
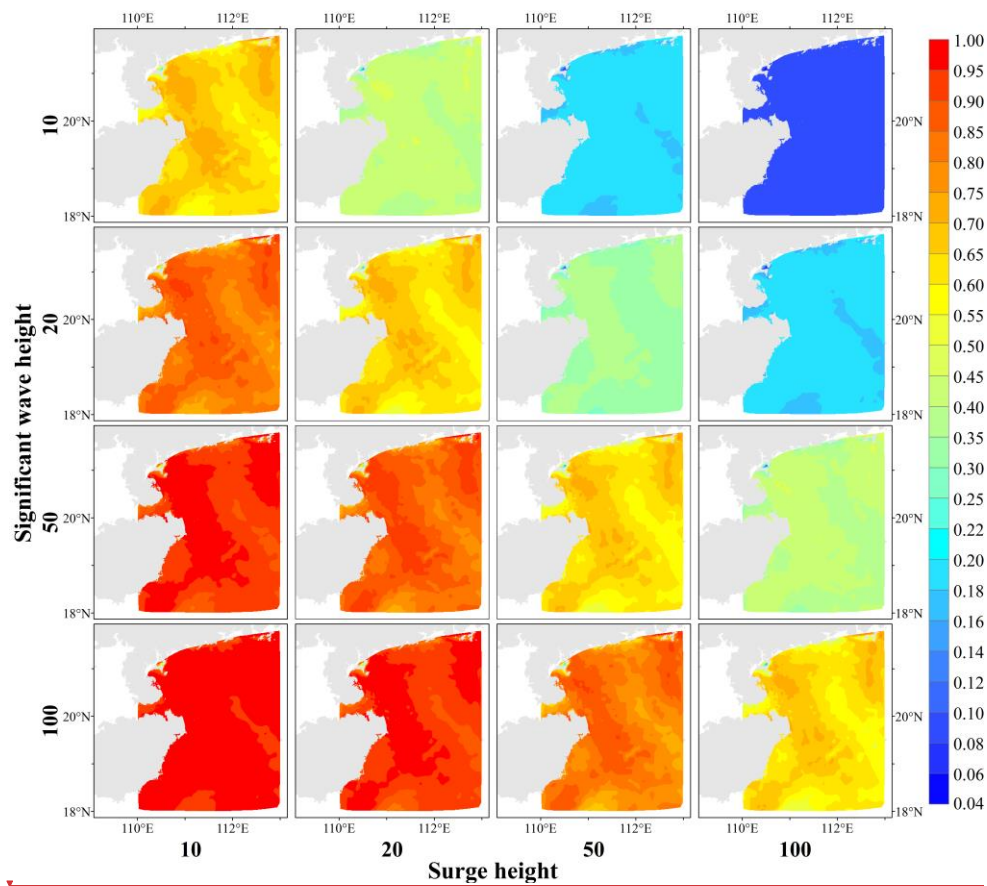
Figure 10: Conditional probabilities of bivariate for different return periods of tropical cyclone significant wave heights
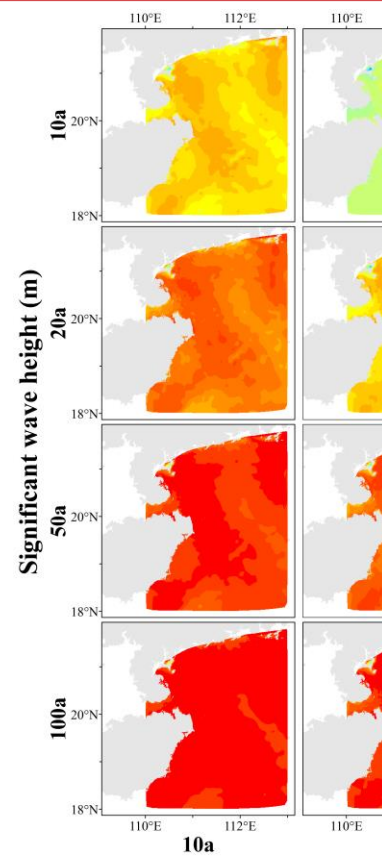
According to the classification criteria of the hazard indicators (Table 2), SH and SWH are divided into five classes. We

700   calculate the combined scenario probability $P_\&$ based on Eq. 12 for all nodes with different combinations of SH and SWH for

a total of 25 scenarios and interpolate them into 1 km raster data using the cubic spline interpolation method (Figure 11).

Regarding the vertical variation pattern, when the SH hazard level is determined, as the SWH hazard level increases, the high-

value area of the combined scenario probability gradually moves away from the coastline, and the scope of the nearshore low-

value area gradually expands. This result is consistent with the geographic distribution pattern: the SWH is low nearshore and

705   high offshore. In the horizontal variation pattern, when the SWH hazard level is determined, as the SH hazard level increases,

the range of low-value areas for the combined scenario probabilities expand, and the low-value area's left boundary gradually

approaches the coastline. This result is consistent with the geographic distribution of SHs being high nearshore and low

offshore. Overall, the maximum value of the probability for each combined scenario tends to decrease as the hazard level of

SH or SWH increases. The larger SH and SWH are concentrated in the eastern Leizhou Peninsula at a certain distance from

710   the coast, with other areas less likely to occur.
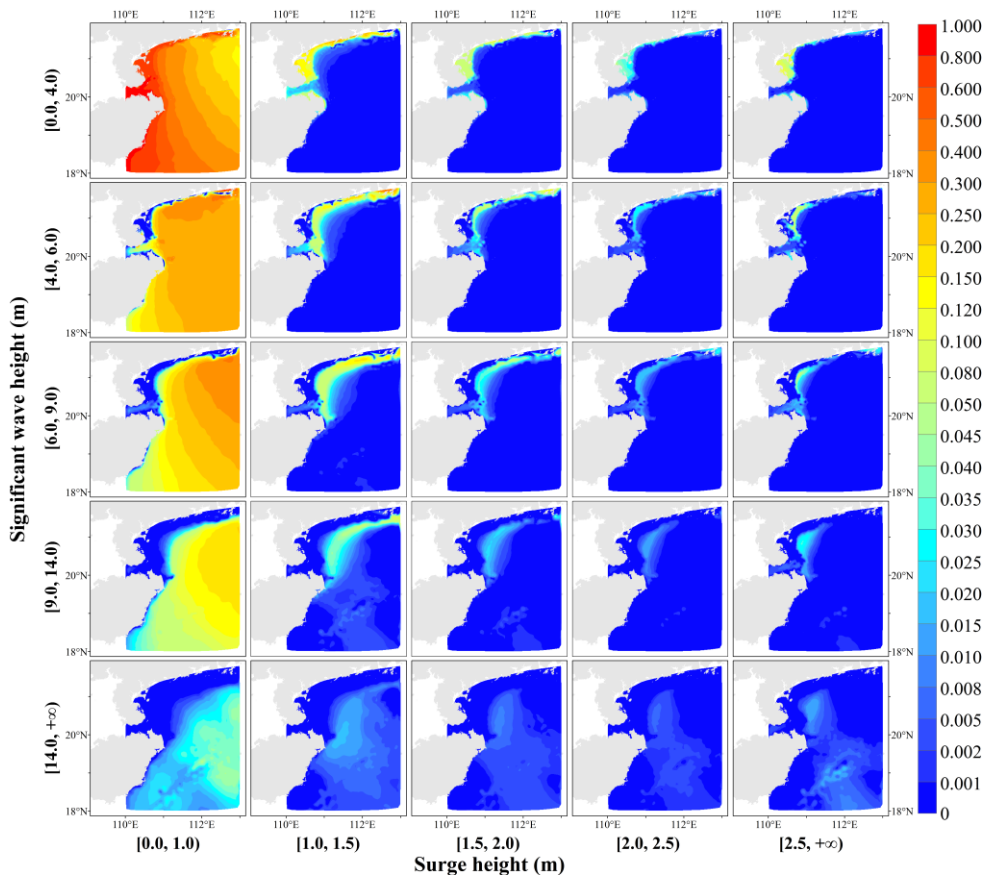
Figure 11: Probabilities of combined scenarios with different levels of surge height and significant wave height for tropical cyclones

Based on the calculated $P_{\cap}$, $P_{\cup}$, $P_{|}$, and $P_{\&}$ with different return periods, Markov chain Monte Carlo (MCMC) and other methods can be further applied to generate random samples for quantitatively assessing TC storm surges and waves. On the other hand, we can explore the effect of varying the intensity values of SH and SWH on the bivariate joint probabilities and apply it to the engineering design criteria.

4.5 Design storm surge and wave criteria

In the design of the engineering fortification criteria, if one hazard indicator is dominant, upgrading the return period for the other variable can effectively change bivariate $P_\cap$ and $P_\cup$ when the conditions for their return period fortification criteria are determined. In this paper, we calculate the change in probability based on Eq. 13, Eq. 14, and Eq. 15 to determine the shift in the probability that remains constant when the positions of the two hazard indicators are switched. Therefore, we calculate the change values in $P_\cap$, $P_\cup$, and $P_|$ for all nodes when the design return period criterion for a given variable is increased from 5-year, 10-year, 20-year, and 50-year to 10-year, 20-year, 50-year, and 100-year respectively. And the data are interpolated into 1 km raster data using the cubic spline interpolation method (Figure 12, Figure 13, and Figure 14).

Figure 12 shows the distribution of the reduction values of bivariate $P_\cap$ for the scenario with elevated univariate return period protection criteria. As the return period protection criteria of one variable increase, the decline in $P_\cap$ gradually decreases as the return period of the other variable's protection standard increases. Its reduction is concentrated between 0 and 0.035. When the return period protection standard of one variable is fixed, as the protection criteria of another variable are gradually increased, the decline of $P_\cap$ rises to a certain level and then tends to decrease. When the return period of one variable is 10-year or 20-year, the decline in $P_\cap$ increases when the protection standard of another variable is raised. If the design criteria increase from a 50-year to a 100-year return period, the change value of $P_\cap$ decreases.
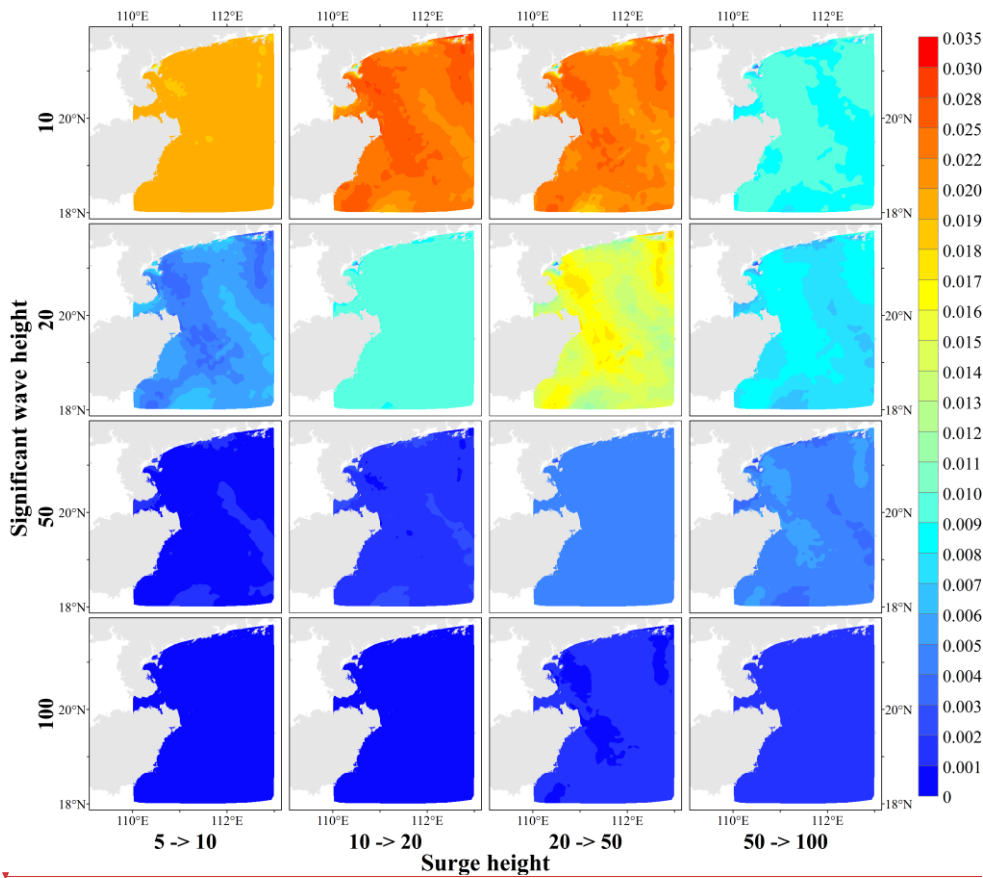
Figure 12: Difference in the simultaneous probability of tropical cyclone surge height and significant wave height for scenarios with elevated return period protection standards
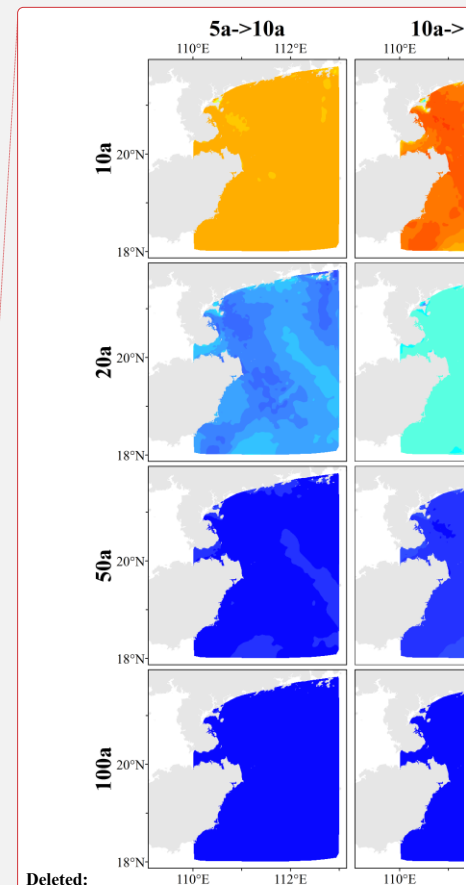
760 Figure 13 shows the distribution of the reduced values for bivariate $P_\cup$ when the protection criteria for the univariate return period is increased. Among them, $P_\cup$ decreases more than $P_\cap$, and the reduced value of $P_\cup$ varies from 0 to 0.105. As the return period protection standard for one variable gradually increases, $P_\cup$ slowly decreases after the protection criteria for the other variable increase. When the return period protection criterion for one variable is fixed, the decline in $P_\cup$ gradually

decreases as the design criteria for the other variable are increased.
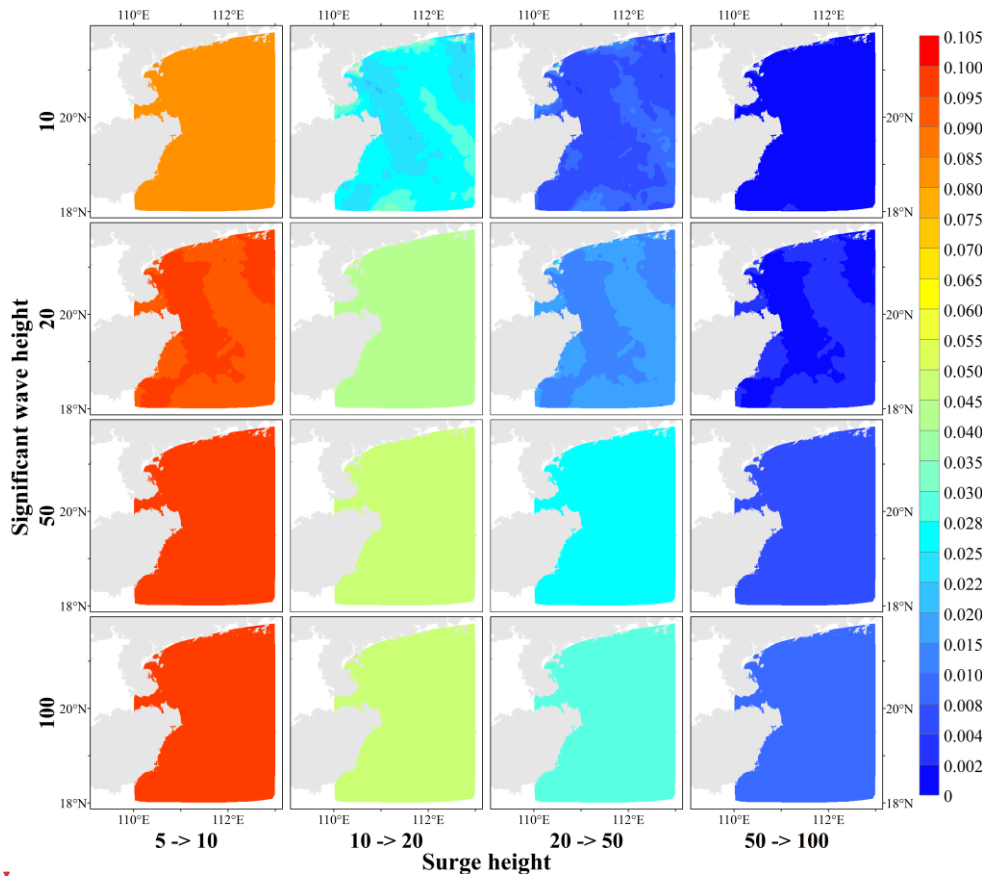
Figure 13: Difference in joint probability of tropical cyclone surge height and significant wave height for scenarios with elevated return period protection standards

770

Figure 14 shows the distribution of the reduced values of bivariate $P_|$ for the scenario of raising the univariate return period protection criteria. As the return period for one variable increases, there is a decreasing trend in the decrease in $P_|$ after the design criteria for the other variable are raised. $P_|$ has a more significant decrease than $P_\cap$ and $P_\cup$, and the decreasing value
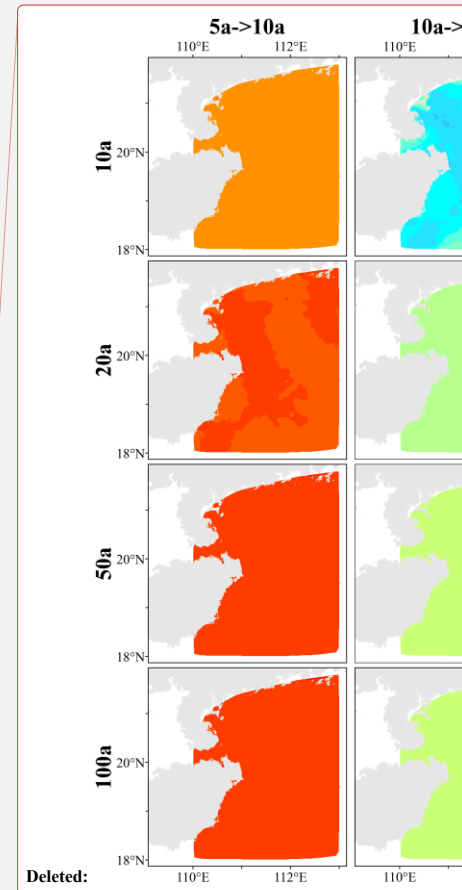
of $P_|$ varies from 0 to 0.45. When the protection level of one variable is fixed and low, the reduction in $P_|$ will tend to decrease after the design criteria of another variable are raised to a certain level. When the protection standard for one variable is a 10-year or 20-year return period, the decrease in bivariate $P_|$ tends to increase when the design criterion for the other variable's return period is raised, but the decrease in $P_|$ is slightly reduced when the design criterion of the other variable is increased from a 50-year to a 100-year return period. If the protection level of one variable is high, the decrease in $P_|$ after the protection standard of the other variable is raised always tends to increase.

780
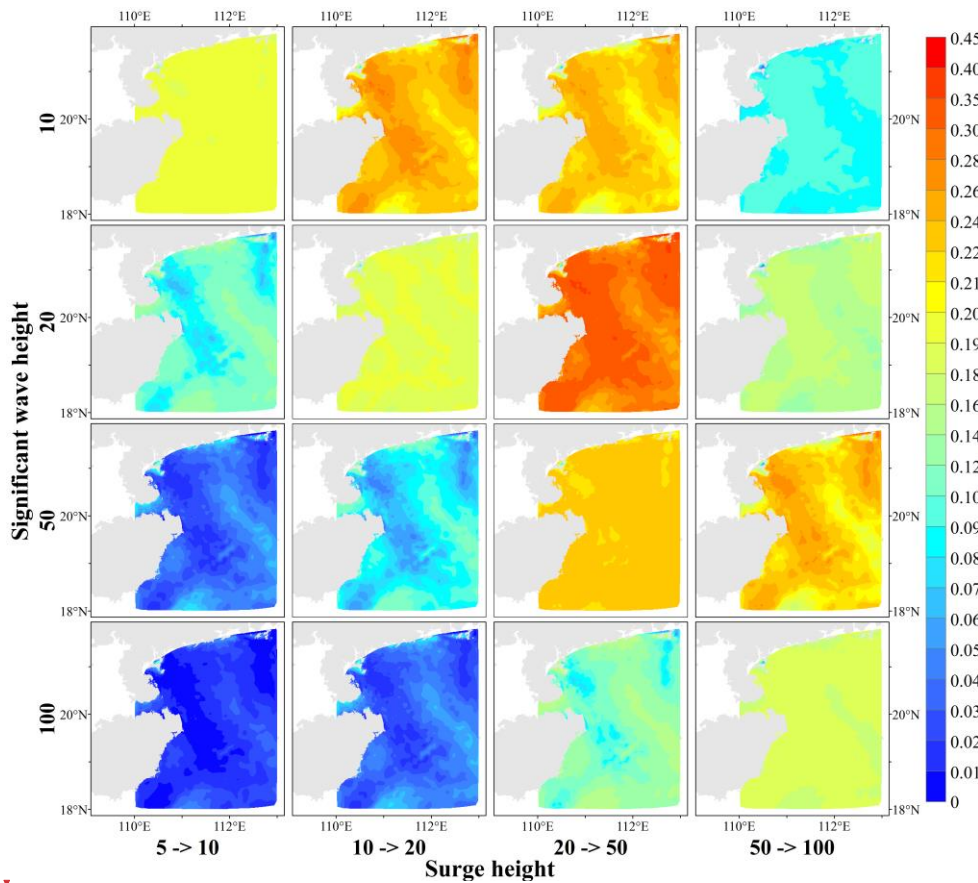
Figure 14: Differences in the conditional probability of tropical cyclone surge height and significant wave height for scenarios with elevated return period protection standards
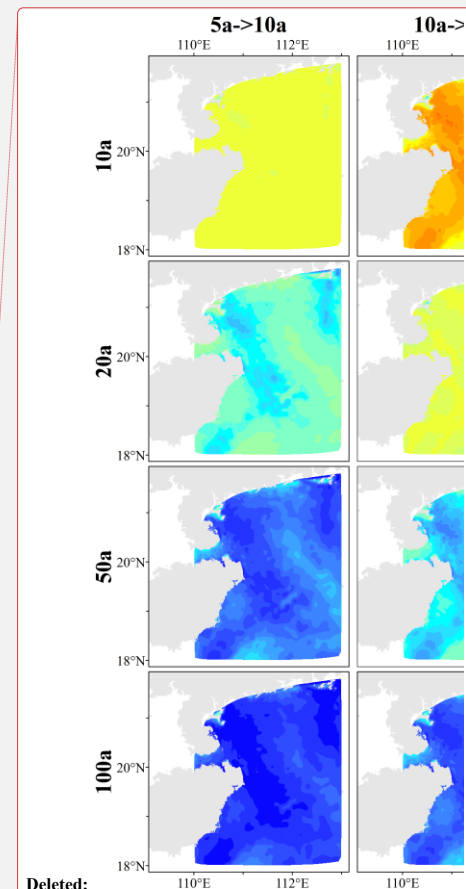
790   In the engineering design criteria, the appropriate design surge height and significant wave height are set according to the bivariate RP_U and $RP_\cap$, the estimation method is shown in Section 3.4.2. In this paper, the design values of SH and SWH for six RP_U for all nodes are calculated based on the above method and interpolated to 1 km raster data by the cubic spline interpolation method (Figure 15 and Figure 16). The design criteria for SH and SWH show an apparent increasing trend as the

return period increases, with the high-value area for SH constantly concentrated east of the Leizhou Peninsula and the high-value area for SWH concentrated in the east of Hainan Island.

When RP_U is a 5-year return period, the design criteria of SH are between 1.5 m and 2.5 m in the eastern coastal area of the Leizhou Peninsula and fall below 0.5 m in the southeastern coastal region of Hainan Island. As the return period increases, the design surge height gradually increases, and when RP_U is a 200-year return period, the design surge height in the eastern coastal area of the Leizhou Peninsula is generally higher than 3.0 m. The design surge height in the northeast coastal area of Hainan Island is mainly between 3.0 m and 15.0 m, while that in the southeast coastal region of Hainan Island is between 0.5 m and 2.0 m, which is lower than that in the northeast.
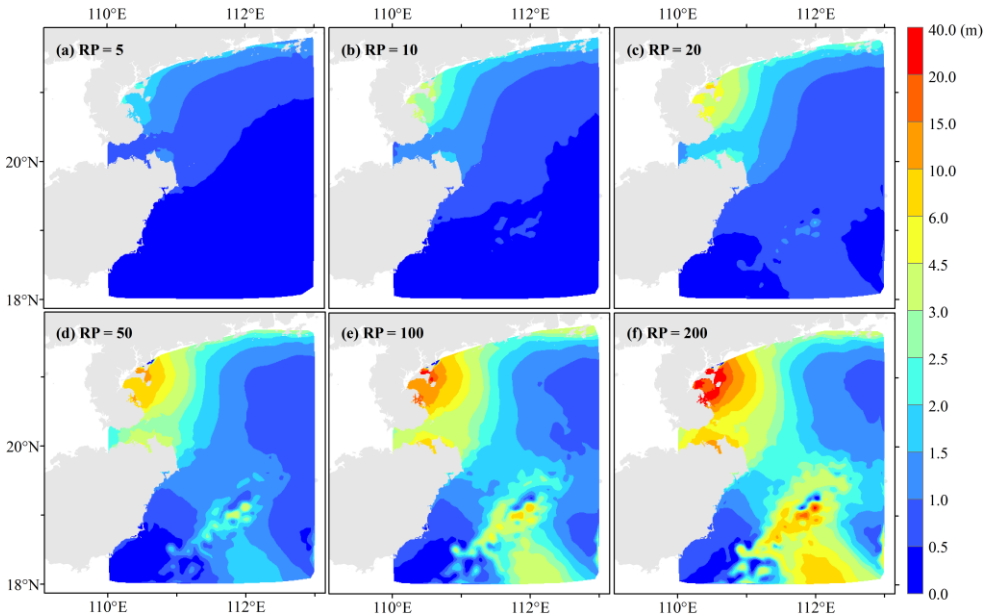
Figure 15: Design surge heights for six typical joint return period scenarios

When RP_U is a 5-year return period, the design criteria of SWH in the coastal areas of the Leizhou Peninsula and Hainan Island are less than 2.5 m overall. The further from the coastline, the protection standard gradually increases. As the return

period increases, the design criteria of SWH gradually increase, and the growth is more evident than that of SH. When RP_U

is a 200-year return period, SWH along the coast of the Leizhou Peninsula is generally less than 6.0 m, while the design SWH

along the Qiongzhou Strait and southeastern Hainan Island is relatively high.
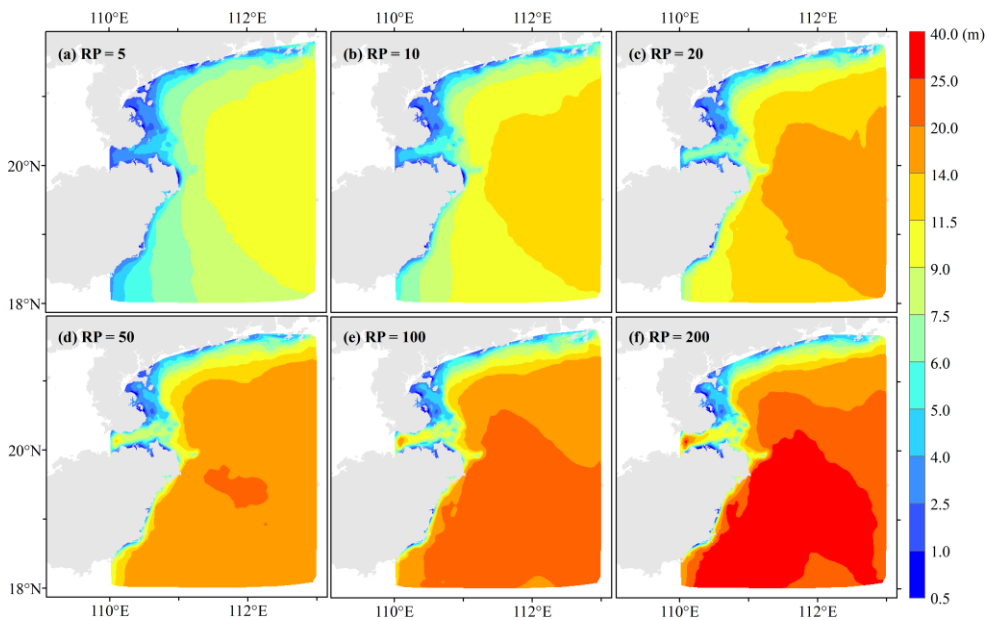
Figure 16: Design significant wave heights for six typical joint return period scenarios

5 Conclusions

In this study, we aimed to estimate joint probability analysis on storm surge and waves using Copula functions on a large

dataset from a wide area and determine their respective design standards as scalar values of SWH and SH. Our main

conclusions are as follows:

1) The GEV function is the most suitable for the probability distribution characteristics of the annual extremes of tropical

cyclone SH and SWH for all nodes in the study area. The Gumbel Copula function is appropriate as a bivariate joint distribution

830   function for all nodes in the study area.

2) The hazard of a single indicator can be characterized by the univariate intensity values with different return periods, which the optimal marginal function can estimate. Our findings show that the SH exhibits a significant increasing trend closer to the coastline, while SWH is higher farther from the shoreline across different return periods. However, we also observe apparent spatial heterogeneity in the distribution, influenced by factors such as the shoreline shape, coastal and submarine topography,

835   and deflection forces.

3) Bivariate probabilities are utilized in this study to assess the integrated hazard of multiple indicators, including $P_\cap$, $P_\cup$, $P_|$, and $P_\&$, which effectively compensates for the deficiency of disregarding the correlation among variables in univariate hazard assessment. These four probabilities can visually describe the occurrence probability for different combinations of scenarios; the more significant the probability is, the higher the hazard. Overall, $P_|$ is the largest, $P_\cup$ is the second largest, and $P_\cap$ is

840   the smallest, while $P_\&$ is influenced by the classification of single hazard indicators. When one variable is constant, $P_\cap$, $P_\cup$, and $P_|$ tend to decrease as the return period of the other variable increases.

4) In actual design criteria, the bivariate $P_\cap$, $P_\cup$, and $P_|$ can be reduced by appropriately increasing the design surge height and significant wave height. When the return period protection standard of one variable is fixed, as the design criteria of another variable gradually increase, the decline in $P_\cap$ and $P_|$ rises to a certain level and then tends to decrease, but the decline

845   in $P_\cup$ gradually decreases. Therefore, developing appropriate design criteria for the SHs and SWHs can effectively reduce the impact of tropical cyclone marine hazards in coastal areas. Since the joint probability distribution of the bivariate is a three-dimensional surface, to obtain specific scalar values for these two hazards as design criteria, in this study, the optimal design criteria for storm surge and waves under the objective of minimum bivariate simultaneous return period are estimated using a non-linear programming approach with their estimated joint return periods as constraints.

850   Although this study provides helpful insights into joint probability analysis of storm surges and waves using Copula functions, several limitations need to be addressed in future research. One limitation is the absence of water level rise caused by storm surges in the numerical modeling of waves, which may introduce errors in the simulation of SWHs in intermediate and shallow water. In addition, exploring the contribution of other indicators, such as long-term sea level rise as environmental hazards, can further improve the accuracy of risk assessment.

Author contributions. FWH and ZHX conceived the research framework and developed the methodology. ZHX was responsible for the code compilation, data analysis, graphic visualization, and first draft writing. FWH managed the implementation of research activities and revised the manuscript. CM participated in the data collection of this study. All authors discussed the results and contributed to the final version of the paper.

Competing interests. The authors declare that they have no conflict of interest.

Acknowledgments. This work was mainly supported by the National Key Research and Development Program of China (grant nos. 2017YFA0604903 and 2018YFC1508803) and the Key Special Project for Introduced Talents Team of Southern Marine Science and Engineering Guangdong Laboratory (Guangzhou) (grant no. GML2019ZD0601). We are grateful to Xing Liu of the Ocean University of China for providing the simulation data of storm surges and waves for historical tropical cyclone events.

Financial support. This research has been supported by the National Key Research and Development Program of China (grant nos. 2017YFA0604903 and 2018YFC1508803), and the Key Special Project for Introduced Talents Team of Southern Marine Science and Engineering Guangdong Laboratory (Guangzhou) (grant no. GML2019ZD0601).

References

Bazaraa, M. S., Sherali, H. D., and Shetty, C. M.: Nonlinear programming: Theory and algorithms, Third Edit., John Wiley & Sons, Ltd, Hoboken, New Jersey, 872 pp., https://doi.org/https://doi.org/10.1002/0471787779, 2006.

Bilskie1, M. V., Hagen, S. C., Medeiros, S. C., Cox, A. T., Salisbury, M., and Coggin, D.: Data and numerical analysis of astronomic tides, wind-waves, and hurricane storm surge along the northern Gulf of Mexico, J. Geophys. Res. Ocean., 121, 3625–3658, https://doi.org/10.1002/2015JC011400, 2016.

Bomers, A., Schielen, R. M. J., and Hulscher, S. J. M. H.: Consequences of dike breaches and dike overflow in a bifurcating river system, Nat. Hazards, 97, 309–334, https://doi.org/10.1007/s11069-019-03643-y, 2019.

Brown, J. M.: A case study of combined wave and water levels under storm conditions using WAM and SWAN in a shallow water application, Ocean Model., 35, 215–229, https://doi.org/10.1016/j.ocemod.2010.07.009, 2010.

Chen, L. and Guo, S.: Copulas and its application in hydrology and water resources, First Edit., Springer Singapore, Singapore, 290 pp., https://doi.org/10.1007/978-981-13-0574-0, 2019.

Chen, Y. and Yu, X.: Sensitivity of storm wave modeling to wind stress evaluation methods, J. Adv. Model. Earth Syst., 9, 893–907, https://doi.org/10.1002/2016MS000850, 2017.

Chen, Y., Li, J., Pan, S., Gan, M., Pan, Y., Xie, D., and Clee, S.: Joint probability analysis of extreme wave heights and surges along China's coasts, Ocean Eng., 177, 97–107, https://doi.org/10.1016/j.oceaneng.2018.12.010, 2019.

Corbella, S. and Stretch, D. D.: Simulating a multivariate sea storm using Archimedean copulas, Coast. Eng., 76, 68–78, https://doi.org/10.1016/j.coastaleng.2013.01.011, 2013.

Dietrich, J. C., Tanaka, S., Westerink, J. J., Dawson, C. N., Luettich, R. A., Zijlema, M., Holthuijsen, L. H., Smith, J. M., Westerink, L. G., and Westerink, H. J.: Performance of the unstructured-mesh, SWAN+ ADCIRC model in computing hurricane waves and surge, J. Sci. Comput., 52, 468–497, https://doi.org/10.1007/s10915-011-9555-6, 2012.

Galiatsatou, P. and Prinos, P.: Joint probability analysis of extreme wave heights and storm surges in the Aegean Sea in a changing climate, E3S Web Conf., 7, 1–12, https://doi.org/10.1051/e3sconf/20160702002, 2016.

Hsu, C. H., Olivera, F., and Irish, J. L.: A hurricane surge risk assessment framework using the joint probability method and surge response functions, Nat. Hazards, 91, S7–S28, https://doi.org/10.1007/s11069-017-3108-8, 2018.

Huang, Y., Weisberg, R. H., Zheng, L., and Zijlema, M.: Gulf of Mexico hurricane wave simulations using SWAN: Bulk formula-based drag coefficient sensitivity for Hurricane Ike, J. Geophys. Res. Ocean., 118, 3916–3938, https://doi.org/10.1002/jgrc.20283, 2013.

Hughes, S. A. and Nadal, N. C.: Laboratory study of combined wave overtopping and storm surge overflow of a levee, Coast. Eng., 56, 244–259, https://doi.org/10.1016/j.coastaleng.2008.09.005, 2009.

Jang, J. H. and Chang, T. H.: Flood risk estimation under the compound influence of rainfall and tide, J. Hydrol., 606, 127446, https://doi.org/10.1016/j.jhydrol.2022.127446, 2022.

Kimf, K. O., Yuk, J., Leen, H. S., and Choi, B. H.: Typhoon Morakot induced waves and surges with an integrally coupled tide-surge-wave finite element model, J. Coast. Res., 2, 1122–1126, https://doi.org/10.2112/S175-225.1, 2016.

Lee, D. Y. and Jun, K. C.: Estimation of design wave height for the waters around the Korean Peninsula, Ocean Sci. J., 41, 245–254, https://doi.org/10.1007/BF03020628, 2006.

Lee, T., Modarres, R., and Ouarda, T. B. M. J.: Data-based analysis of bivariate copula tail dependence for drought duration and severity, Hydrol. Process., 27, 1454–1463, https://doi.org/10.1002/hyp.9233, 2013.

Li, J., Fang, W., Zhang, X., Cao, S., Yang, X., Liu, X., and Sun, J.: Similar tropical cyclone retrieval method for rapid potential storm surge and wave disaster loss assessment based on multiple hazard indictors, Mar. Sci., 40, 49–60, https://doi.org/10.11759/hykx20151104001, 2016.

Li, L., Pan, Y., Amini, F., and Kuang, C.: Full scale study of combined wave and surge overtopping of a levee with RCC strengthening system, Ocean Eng., 54, 70–86, https://doi.org/10.1016/j.oceaneng.2012.07.021, 2012.

Lin, N., Emanuel, K. A., Smith, J. A., and Vanmarcke, E.: Risk assessment of hurricane storm surge for New York City, J. Geophys. Res. Atmos., 115, 1–11, https://doi.org/10.1029/2009JD013630, 2010.

Liu, X., Jiang, W., Yang, B., and Baugh, J.: Numerical study on factors influencing typhoon-induced storm surge distribution in Zhanjiang Harbor, Estuar. Coast. Shelf Sci., 215, 39–51, https://doi.org/10.1016/j.ecss.2018.09.019, 2018.

Lu, X., Yu, H., Ying, M., Zhao, B., Zhang, S., Lin, L., Bai, L., and Wan, R.: Western North Pacific Tropical Cyclone Database Created by the China Meteorological Administration, Adv. Atmos. Sci., 38, 690–699, https://doi.org/10.1007/s00376-020-0211-7, 2021.

Marcos, M., Rohmer, J., Vousdoukas, M. I., Mentaschi, L., Le Cozannet, G., and Amores, A.: Increased extreme coastal water

levels due to the combined action of storm surges and wind waves, Geophys. Res. Lett., 46, 4356–4364, https://doi.org/10.1029/2019GL082599, 2019.

MNR: Technical directives for risk assessment and zoning of marine disaster--Part 1: Storm surge, 2019.

MNR: Technical directives for risk assessment and zoning of marine disaster--Part 2: Wave, Beijing, 1–30 pp., 2021.

Morellato, D. and Benoit, M.: Constitution of a numerical wave data-base along the French Mediterranean coasts through hindcast simulations over 1979-2008, Chart, 1–8, https://doi.org/10.13140/2.1.1794.3049, 2010.

Muraleedharan, G., Rao, A. D., Kurup, P. G., Nair, N. U., and Sinha, M.: Modified Weibull distribution for maximum and significant wave height simulation and prediction, Coast. Eng., 54, 630–638, https://doi.org/10.1016/j.coastaleng.2007.05.001, 2007.

Nelsen, R. B.: An intruduction to copulas, Second Edi., Springer Science+Business Media, New York, 1–656 pp., 2006.

Niedoroda, A. W., Resio, D. T., Toro, G. R., Divoky, D., Das, H. S., and Reed, C. W.: Analysis of the coastal Mississippi storm surge hazard, Ocean Eng., 37, 82–90, https://doi.org/10.1016/j.oceaneng.2009.08.019, 2010.

Pan, Y., Li, L., Amini, F., and Kuang, C.: Full-scale HPTRM-strengthened levee testing under combined wave and surge overtopping conditions: Overtopping hydraulics, shear stress, and erosion analysis, J. Coast. Res., 29, 182–200, https://doi.org/10.2112/JCOASTRES-D-12-00010.1, 2013.

Pan, Y., Zhang, Z., Yuan, S., Zhou, Z., and Chen, Y.: An overview of research on combined wave and surge overtopping on levees, Adv. Sci. Technol. Water Resour., 39, 90–94, https://doi.org/10.3880/j.issn.1006-7647.2019.01.015, 2019.

Papadimitriou, A. G., Chondros, M. K., Metallinos, A. S., Memos, C. D., and Tsoukala, V. K.: Simulating wave transmission in the lee of a breakwater in spectral models due to overtopping, Appl. Math. Model., 88, 743–757, https://doi.org/10.1016/j.apm.2020.06.061, 2020.

Perk, L., van Rijn, L., Koudstaal, K., and Fordeyn, J.: A rational method for the design of sand dike/dune systems at sheltered sites; Wadden Sea Coast of Texel, the Netherlands, J. Mar. Sci. Eng., 7, 1–25, https://doi.org/10.3390/jmse7090324, 2019.

Petroliagkis, T. I., Voukouvalas, E., Disperati, J., and Bidlot, J.: Joint probabilities of storm surge, significant wave height and river discharge components of coastal flooding events. Utilising statistical dependence methodologies and techniques, Publications Office of the European Union, Luxembourg, 79 pp., https://doi.org/10.2788/677778, 2016.

Rao, X., Li, L., Amini, F., and Tang, H.: Numerical study of combined wave and surge overtopping over RCC strengthened levee systems using the smoothed particle hydrodynamics method, Ocean Eng., 54, 101–109, https://doi.org/10.1016/j.oceaneng.2012.06.024, 2012.

Serinaldi, F.: Dismissing return periods!, Stoch. Environ. Res. Risk Assess., 29, 1179–1189, https://doi.org/10.1007/s00477-014-0916-1, 2015.

Shi, X., Han, Z., Fang, J., Tan, J., Guo, Z., and Sun, Z.: Assessment and zonation of storm surge hazards in the coastal areas of China, Nat. Hazards, 100, 39–48, https://doi.org/10.1007/s11069-019-03793-z, 2020.

Sklar, A.: Random variables, joint distribution functions, and copulas, Kybernetika, 9, 449–460, 1973.

Teena, N. V., Sanil Kumar, V., Sudheesh, K., and Sajeev, R.: Statistical analysis on extreme wave height, Nat. Hazards, 64, 223–236, https://doi.org/10.1007/s11069-012-0229-y, 2012.

Trepanier, J. C., Needham, H. F., Elsner, J. B., and Jagger, T. H.: Combining surge and wind risk from hurricanes using a copula model: An example from Galveston, Texas, Prof. Geogr., 67, 52–61, https://doi.org/10.1080/00330124.2013.866437,

2015.

Wahl, T., Mudersbach, C., and Jensen, J.: Assessing the hydrodynamic boundary conditions for risk analyses in coastal areas: A multivariate statistical approach based on Copula functions, Nat. Hazards Earth Syst. Sci., 12, 495–510, https://doi.org/10.5194/nhess-12-495-2012, 2012.

970 Wahl, T., Jain, S., Bender, J., Meyers, S. D., and Luther, M. E.: Increasing risk of compound flooding from storm surge and rainfall for major US cities, Nat. Clim. Chang., 5, 1093–1097, https://doi.org/10.1038/nclimate2736, 2015.

Xie, D. mei, Zou, Q. ping, and Cannon, J. W.: Application of SWAN+ADCIRC to tide-surge and wave simulation in Gulf of Maine during Patriot's Day storm, Water Sci. Eng., 9, 33–41, https://doi.org/10.1016/j.wse.2016.02.003, 2016.

Xu, H., Tan, J., Li, M., and Wang, J.: Compound flood risk of rainfall and storm surge in coastal cities as assessed by copula

975 formal, J. Nat. Disasters, 31, 40–48, https://doi.org/10.13577/j.jnd.2022.0104, 2022.

Zhang, B. and Wang, S.: Probabilistic characterization of extreme storm surges induced by tropical cyclones, J. Geophys. Res. Atmos., 126, 1–22, https://doi.org/10.1029/2020JD033557, 2021.